Integrated high temperature longitudinal, shear and plate acoustic wave transducers

Kobayashi, Makiko; Jen, Cheng-Kuei; Ono, Yuu; Wu, Kuo-Ting; Shih, Ishang

Publisher's version / Version de l'éditeur:
https://doi.org/10.1143/JJAP.46.4688
Japanese Journal of Applied Physics, 46, 7B, pp. 4688-4692, 2007-07-26

Integrated High Temperature Longitudinal, Shear, and Plate Acoustic Wave Transducers

Makiko Kobayashi[†1], Cheng-Kuei Jen[1], Yuu Ono[1], Kuo-Ting Wu[2] and Ishang Shih[2]

[1] Industrial Materials Institute, National Research Council Canada

75 de Mortagne Blvd., Boucherville, QC, J4B 6Y4, Canada

[2]Department of Electrical and Computer Engineering

3480 University Street, Montreal, QC, H3A 2K6, Canada

Abstract

Thick (>40μm) ceramic films as piezoelectric ultrasonic transducers (UTs) have been successfully deposited on metallic substrates by a spray technique. In the film fabrication a composite consisting of piezoelectric powders well mixed with solution of high dielectric constant is directly sprayed onto the substrate. It is then dried, fired or annealed by heat. Multiple coating is used to achieve desired film thicknesses. A corona poling is utilized to achieve the piezoelectricity of the film. The top electrode is accomplished by painting, spray coating, or vacuum evaporation of appropriate electrode materials. All fabrication processes can be carried out on-site and by handheld devices. Integrated ultrasonic longitudinal, shear, and plate wave transducers have been made. These transducers have been tested and operated at 350°C.

Keywords: High temperature ultrasonic measurement, Rayleigh wave transducer, Lamb wave transducer, longitudinal wave transducer, shear wave transducer, interdigital transducer, integrated ultrasonic transducer, nondestructive testing

1. Introduction

Due to the simplicity, speed, economy and capability to probe the interior of an opaque material, ultrasonic techniques are often used to perform nondestructive testing and characterization (NDT&C) of materials [1,2]. Many NDT&C are also mandatory to be performed at elevated temperatures, thus high temperature (HT) ultrasonic transducers (UTs) are in demand [3-7]. For applications of smart structures and materials there is also a critical need for integrated in-situ sensors for local and global damage detection and assessment. The purpose of this investigation is to demonstrate the fabrication of integrated HT longitudinal (L), shear (S) and surface (or plate) acoustic wave transducers directly onto desired structures or materials for NDT&C applications.

2. Fabrication and Characterization

In this study thick (>40μm) piezoelectric ceramic films as UTs are of interest. These films are made by a sol-gel spray technique [5,7]. The ball-milled sub-micron piezoelectric bismuth titanate (BIT) powders were dispersed into lead zirconate titanate (PZT) sol-gel solution. The BIT and PZT were chosen because of its high Curie temperature (675°C) and high dielectric constant, respectively. The final BIT/PZT mixture (paint) was then sprayed directly onto selected metallic substrates, such as steel or stainless steel (SS), through an airbrush. With this sol-gel spray technique, the films can be produced at desired locations using a paper shadow mask. After spraying the coating, thermal treatments such as drying, firing and annealing were carried out using a heat gun or a furnace. Multiple coatings were made in order to reach desired film thicknesses. In this study the film thickness is between 40 and 120μm. The BIT/PZT films were then electrically poled using a corona discharging technique. The corona poling method was chosen because it could pole the piezoelectric film over a large area with complex

geometries. Finally, silver paste, platinum paste or vacuum evaporation method was used to form the top electrodes at room temperature.

The measured relative dielectric constant of the BIT/PZT film was about 80. The d_{33} measured by an optical interferometer was 10×10^{-12} m/V.

3. Shear and Longitudinal Wave Probes

Various efforts have been devoted to develop L wave HTUTs of large bandwidth and high efficiency [3-7], which have been supplied by several companies. However, it is understood that S waves may be advantageous over L waves for NDT and characterization of materials because liquid and gas medium do not support S waves. In addition, for the evaluation of material properties, sometimes it is important to measure shear modulus and viscoelastic properties in which S wave properties are a requisite. Furthermore, a HTUT setup to generate and receive both L and S waves at the same sensor location would be also of interest.

The mode conversion from L to S wave due to reflection at a solid-air interface was reported in refs. [8,9]. It means that the L wave UT together with L-S mode conversion can be effectively used as a S wave probe as shown in Fig.1. In Fig.1, L_i waves generated by an L wave UT reach a solid-air interface and reflected as L_r and S_r waves. The equations governing the reflection and mode conversion with respect to the L wave incident angle θ can be given in eqs. (1)-(3) [10], where ϕ is reflection angle of the S waves, V_l and V_s are L and S wave velocities in the solid, respectively, and R_{ll} and R_{sl} are energy reflection coefficients of the L and S waves, respectively.

$$\frac{V_l}{\sin\theta} = \frac{V_s}{\sin\varphi} \qquad (1)$$

$$R_{ll} = \left[\frac{\cos^2 2\varphi - (V_s/V_l)^2 \cdot \sin 2\theta \cdot \sin 2\varphi}{\cos^2 2\varphi + (V_s/V_l)^2 \cdot \sin 2\varphi \cdot \sin 2\theta} \right]^2 \quad (2)$$

$$R_{sl} = \frac{4(V_s/V_l)^2 \cdot \cos^2 2\varphi \cdot \sin 2\theta \cdot \cos 2\varphi}{\left[\cos^2 2\varphi + (V_s/V_l)^2 \cdot \sin 2\varphi \cdot \sin 2\theta\right]^2} \quad (3)$$

In this study, a mild steel with V_l = 5900 m/s and V_s = 3200 m/s at room temperature was used as the substrate. Fig.2 shows the calculated energy reflection coefficients of R_{ll} (dotted line) and R_{sl} (solid line) based on eqs. (2) and (3), respectively, at the mild steel-air interface. It indicates that the maximum energy conversion rate from the L_i wave to the S_r wave is 97.5% at θ = 67.2°, and the reduction of the energy conversion rate is within 1% in the θ range between 60.8° and 72.9°.

In order to achieve S wave HTUTs, first we fabricated an L wave UT of a 100μm-thick BIT/PZT film onto a mild steel substrate using the sol-gel spray technique described in Section 2. Let this L UT be in a plane parallel to the mode converted S wave direction as shown in Fig. 3(a). This approach could reduce machining time of the substrate and thick UT film fabrication difficulty. The top electrode was made by a platinum paste which can sustain the temperature up to more than 450°C. By considering this criterion, $\theta + \varphi$ is required to be 90°. From eq. (1), which is the Snell's law, we can obtain θ = 61.5°. At this angle, the L-S conversion rate is 96.7% that is only 0.8% smaller than the maximum conversion rate at 67.2°, based on the result in Fig. 2. Therefore, Figs. 3(a) and 3(b) show the design schematic and actual device developed for this study, respectively. Figures 4(a) and 4(b) show the ultrasonic signal in time and frequency domain, respectively, of the received S_r wave in a pulse-echo mode at 350°C. The S^n represents nth round trip of the S wave echoes traversing back and forth between the L UT and the probing end in Fig. 3. The center frequency of the S^1 echo was 6.7MHz and the 6dB bandwidth was 3.8MHz. The signal-to-noise ratio (SNR) of the S^1 echo was about 30dB. The

SNR is defined as the ratio of the amplitude of the S^1 echo over that of the undesired signals among the S^n echoes in Fig. 4(a). The signal strength of the S^1 echo at 350°C was 5dB smaller than that at room temperature. It can be seen that the L_r wave was not observed due to the fact that the dimension of the substrate has been chosen so that the reflected L_r wave does not enter into the aperture of the L UT.

If one would like to generate and receive both L and S waves at the same time, then the S wave probe shown in Fig. 3 can be modified to achieve such a purpose. In fact, it simply makes a slanted surface with an angle 45° from the intersection of the slanted plane and the line from the center of the L UT as shown in Fig. 5(a). The 45° angle plane will reflect the energy of the L_i wave into the $L_{r,45°}$ wave normal to the probing end as shown in Fig. 5(a). Therefore, in principle, the upper part of the L_i wave, generated from L UT, can be used to produce the S_r wave and the lower part to produce the $L_{r,45°}$ wave. Fig.5(b) shows an actual device developed. Fig.6 shows ultrasonic signal in time domain in the pulse-echo mode at 350 °C, in which the S_r (S^1) and L_r (L^1) waves are observed simultaneously. The L^1 represents the first round trip L_r wave echo traversing between the L UT and the probing end. The center frequencies of the S^1 and L^1 echoes were 7.0MHz and 7.0MHz and the 6dB bandwidths were 3.0 MHz and 3.8MHz, respectively. During the top electrode fabrication for the device shown in Fig. 5(b), the area and position of the top electrode were adjusted so that the amplitude of the reflected S_r and $L_{r,45°}$ waves were nearly the same. The SNRs of the L^1 and S^1 were about 20 dB.

4. Plate Acoustic Waves Transducers

For NDT applications there is a critical need for integrated in-situ sensors for local and global damage detection and assessment [2]. In the past the local aspect of the damage monitoring on metals has been reported [7]. It is known that plate acoustic wave (PAW) transducers [8, 11] can be used for NDT of metals such as steel and SS in the range of several

centimeters or meters depending on the attenuation characteristics of the substrates. In the common practice the L or S wave UTs with a wedge are used to generate and receive the desired PAW with the proper mode conversion through the wedge [1,2]. However, there is a requirement of an ultrasonic couplant between the wedge and the sample under inspection. It is difficult to apply these UTs, wedges and couplants on curved surfaces and at HT. In this section, the purpose is to develop techniques to fabricate of PAW transducers directly onto desired steel and SS substrates for NDT applications at 350°C. Since pulse-echo modes are of interest for NDT applications, the measurement data will be shown for this mode only although measurement data in transmission modes have been also obtained. One goal is to use these structurally integrated sensors for inspection of, for example, in-flight aircraft critical components, thus increasing platform availability and reducing associated maintenance costs.

The fabrication processes of PAW transducers are the same as those of L UT except that the top electrode is made in a shape of interdigital transducer (IDT). Since in this study the desired PAW operation frequency range is between 0.5 and 2.0MHz, a mask used in this study was designed and fabricated by an electrical discharge machining (EDM) method as shown in Fig.7. The top and bottom connection electrodes are called bus-bars, and the other thin electrodes perpendicular to the wave propagation direction are called fingers. The finger widths of the IDT were 0.5mm. The separation among the fingers was also 0.5mm wide. The mask was made of a 0.57mm-thick SS plate. The thickness was chosen so that the mask is flat, has negligible shadow effect during the top electrode fabrication and is reusable.

For PAW experiments a 111μm-thick BIT/PZT composite film [7] was deposited on a 0.702mm-thick SS plate as shown in Fig.8. Then two IDT electrodes were made on the top of the film by the vacuum deposition technique using the IDT mask shown in Fig.7. Their thickness was 0.1μm. Fig.9 shows the measured PAW signals in time domain using the integrated PAW transducer shown in Fig.8 near edge "A" operated in the pulse-echo mode at

350°C. The pass band of the band pass filter in our signal acquisition system was set between 0.5MHz and 2.0MHz. In Fig.9 P_A, P_B , P_{A+B}, P_{2A+B} and P_{A+2B} are the reflected echoes either from the edge "A" or the edge "B" through the corresponding PAW travel paths (distance) of 2A, 2B, 2(A+B), 2(2A+B) and 2(A+2B), respectively. The longest travel distance in this experiment was 594mm (for P_{A+2B}). The echoes of P_A and P_B are weaker than the P_{A+B} because they travel uni-directionally along A or B direction, respectively, but the echo P_{A+B} travel both along "A" and "B" direction and summed at the IDT near the edge "A" when received. Along the longer propagation distance echo strength will be the weaker due to the higher loss in the path. However, the echoes in Fig. 9 show good SNRs. The two edges can be considered as large deep defects (cracks) in practical NDT applications. It means that this integrated PAW transducer can be regarded as an excellent NDT tool at 350°C for sensing defects with the distance as long as 594mm (e.g. P_{A+2B}).

At room temperature the measured PAW group velocity of the device shown in Fig.8 was 2936m/s. The measured V_l and V_s of the SS plate at room temperature were 5828m/s and 3151m/s, respectively. Let $k_l = \omega/V_l$, $k_S = \omega/V_S$, $k = \omega/V$, $\omega = 2\pi f$ and $q = (k^2 - k_l^2)^{1/2}$ and $s = (k^2 - k_s^2)^{1/2}$ where f is the frequency, then the equations governing the anti-symmetric and symmetric mode Lamb waves are given in eqs.(4) and (5), respectively [11].

$$\left(k^2 + s^2\right)^2 \coth\left(qh/2\right) - 4k^2 qs \coth\left(qh/2\right) = 0 \tag{4}$$

$$\left(k^2 + s^2\right)^2 \tanh\left(qh/2\right) - 4k^2 qs \tanh\left(qh/2\right) = 0 \tag{5}$$

Using eqs. (4) and (5), the calculated PAW phase V (in solid lines) and group velocities V_g (in dashed lines) are shown in Fig10. V_R indicates the phase velocity of Rayligh wave on the substrate having semi-infinite thickness. It is found that at the plate thickness h = 0.702mm and f = 1MHz the theoretically calculated V_g for the first anti-symmetric mode a_0 is 3030m/s which agrees well with the measured V_g of 2936m/s. Note that the calculated result does not include

the effect of the BIT/PZT composite film loading. Therefore the PAW shown in Fig.9 is the first anti-symmetrical plate wave mode a_0. Because the BIT/PZT composite film has slower L wave velocity, 2450 m/s (where is 2450m/s come from?), than that of SS plate, 5828 m/s, the 111μm-thick BIT/PZT film will slow down the PAW velocity in the plate region coated with this film [8,11].

The geometry of the PAW transducer, such as thickness of the BIT/PZT film and finger widths of the IDT which affect operating frequency will be investigate in order to excite PAW waves efficiently in the future study. By comparing the measurement data in Fig.9 with those at room temperature it is found that the signal strength was 5dB weaker at 350°C. The measured PAW (a_0) at 350°C was 2754m/s.

5. Conclusions

Thick (>40μm) ceramic films as piezoelectric UTs were deposited on metallic substrates by a spray technique to fabricate longitudinal, shear and plate wave transducers. In the film fabrication a composite consisting of piezoelectric BIT powders well mixed with PZT solution was directly sprayed onto different substrates. It was then dried, fired and annealed by heat. Multiple coating was used to achieve desired thicknesses. A corona poling was used to achieve the piezoelectricity of the film. The top electrode was accomplished by a painting method with silver paste or platinum paste, or by a vacuum deposition technique. All fabrication processes can be carried out on-site and by handheld devices.

Integrated ultrasonic S wave probes were fabricated onto steel substrates with the use of mode conversion from L to S waves. The theoretical calculation indicates that the maximum energy conversion rate from the L to S wave is 97.5% at the L wave incident angle $\theta = 67.2°$, and the reduction of the energy conversion rate is within 1% in the θ range between 60.8° and 72.9°. Let the L UT be made in a plane parallel to the propagation direction of the mode

converted S waves at the θ=61.5°, clean S waves were generated. The reduction of energy conversion rate at θ= 61.5° is only 0.8% smaller than the maximum conversion rate at θ= 67.2°. A probe that can simultaneously generate and receive both L and S waves was also demonstrated. All the above mentioned probes have been made and operated up to 350 °C with a center frequency of 5–7 MHz, 6dB bandwidth of 4–6 MHz, and SNR of more than 20 dB.

The fabrication and ultrasonic performance of integrated PAW transducers directly onto SS substrates for NDT applications at 350°C have been demonstrated. The IDT mask was made by an EDM method. A vacuum evaporation method was used to form the IDT electrodes through the IDT mask. Experimental results show PAW propagation in the first anti-symmetrical mode along a 0.702mm-thick SS plate. The pass band of the filters for PAW was selected between 0.5MHz and 2.0MHz. The measured PAW results agree well with the theoretically calculated values. If the edges of the substrates can be considered as large defects or cracks, measured signals with good SNR demonstrated the NDT capability in a distance of several centimeters or tens of centimeters of these integrated PAW transducers operated at 350°C. Arrays of these transducers can be readily achieved as well.

Acknowledgments

Authors would like to thank J.-F. Moisan, H. Hebert and N. Mrad for their technical assistance. Financial support from Natural Sciences and Engineering Research Council of Canada is acknowledged.

References

1) J. Krautkrämer and H.H. Krautkrämer : *Ultrasonic Testing of Materials* (Springer-Verlag, Berlin, 1990).

2) A.S. Birks, R.E. Green, Jr. and P. McIntire : *Ultrasonic Testing* (ASNT, 1991), 2nd Ed., Vol.7.

3) T. Arakawa, K. Yoshikawa, S. Chiba, K. Muto, and Y Atsuta : Nondestr. Test. Eval. **7** (1992) 263.

4) H. Karasawa, M. Izumi, T. Suzuki, S. Nagai, M. Tamura, and S. Fujimori: J. of Nuclear Science and Technology **37** (2000) 769.

5) M. Kobayashi, T.R. Olding, M. Sayer and C.-K. Jen: Ultrasonics **39** (2002) 675.

6) R. Kazys, A. Voleisis, R. Sliteris, B. Voleisiene, L. Mazeika, P. H. Kupschus, and H. A. Abderrahim: IEEE Sensor J. **6** (2006) 1134.

7) M. Kobayashi and C.-K. Jen : Smart Mat. and Structures **13** (2004) 951.

8) B.A. Auld : *Acoustic Fields and Waves in Solids* **1&2** (John Wiley & Sons, New York, 1973).

9) M.O. Si-Chaib, H. Djelouah, and M. Bocquet : NDT&E International **33** (2000) 91.

10) W.G. Mayer : Ultrasonics **3** (1965) 62.

11) I.A. Viktorov: *Rayleigh and Lamb waves* (Plenum, New York, 1967).

Figure captions

Fig. 1 Reflection and mode conversion with an L wave incidence at a solid-air interface.

Fig. 2 Energy reflection coefficients of R_{ll} (dotted line) and R_{sl} (solid line) vs. L wave incident angle θ at solid (mild steel)-air interface.

Fig. 3 (a) Schematic diagram and (b) actual device of an integrated S wave UT probe with the L wave UT located in a plane parallel to the direction of mode converted S wave at $\theta = 61.5°$.

Fig.4 Ultrasonic signals in (a) time and (b) frequency domain of the S wave UT probe shown in Fig.3 at 350°C.

Fig.5 (a) Schematic diagram and (b) actual device of an integrated L and S wave probe with the L wave UT located in a plane parallel to the direction of S_r wave.

Fig.6 Ultrasonic signals in time domain of the L and S wave UT probe shown in Fig.5 at 350°C.

Fig.7 A mask of an IDT pattern.

Fig.8 A 0.702mm-thick steel plate with a PAW transducer with an IDT electrode operated in pulse-echo mode. The 111μm-thick piezoelectric film was made of a BIT/PZT composite.

Fig.9 Ultrasonic performance of PAW transducer shown in Fig. 8 with an IDT electrode operated in pulse-echo mode at 350°C in time domain. The SS substrate is 0.702mm thick.

Fig. 10 The calculated PAW dispersion curves for the 0.702mm-thick SS plate shown in Fig.8. V_R indicates the phase velocity of Rayligh wave on the substrate having semi-infinite thickness.

Figures

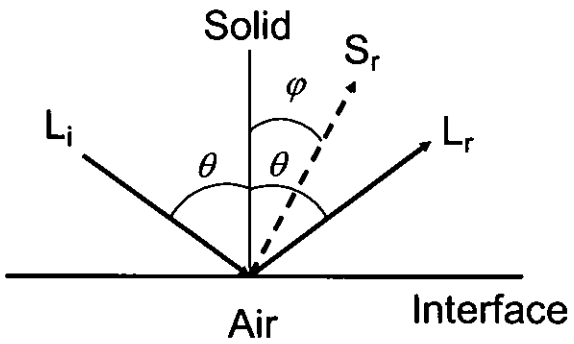

Fig. 1: Makiko Kobayashi, Cheng-Kuei Jen, Yuu Ono, Kuo-Ting Wu and Ishang Shih

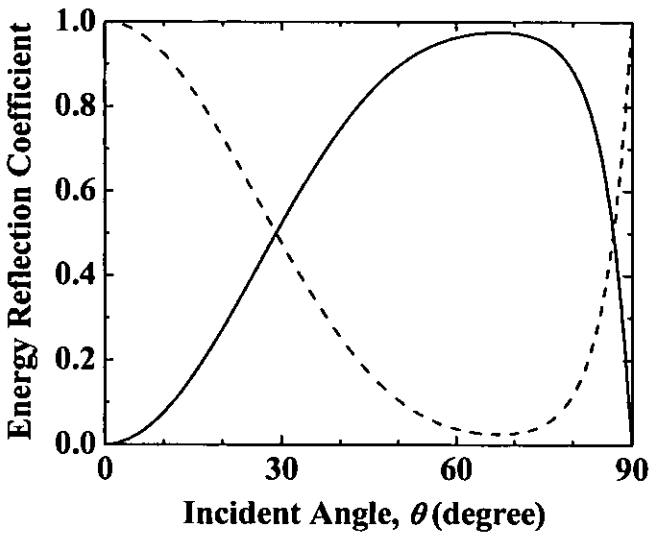

Fig. 2: Makiko Kobayashi, Cheng-Kuei Jen, Yuu Ono, Kuo-Ting Wu and Ishang Shih

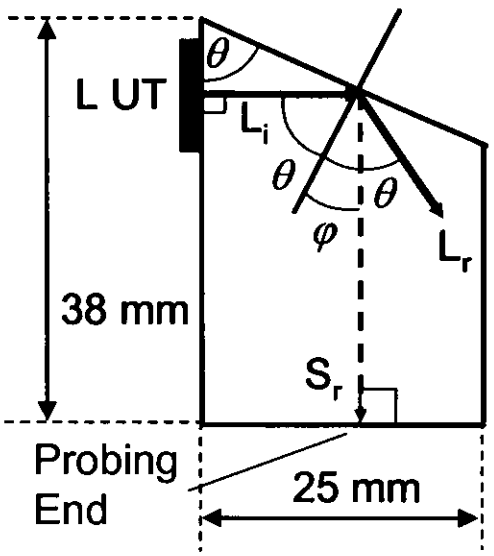

Fig. 3 (a): Makiko Kobayashi, Cheng-Kuei Jen, Yuu Ono, Kuo-Ting Wu and Ishang Shih

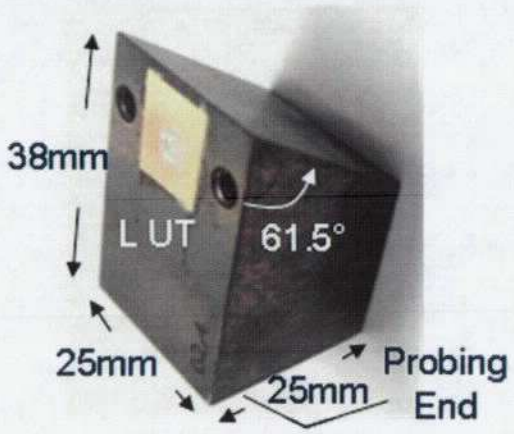

Fig. 3 (b): Makiko Kobayashi, Cheng-Kuei Jen, Yuu Ono, Kuo-Ting Wu and Ishang Shih

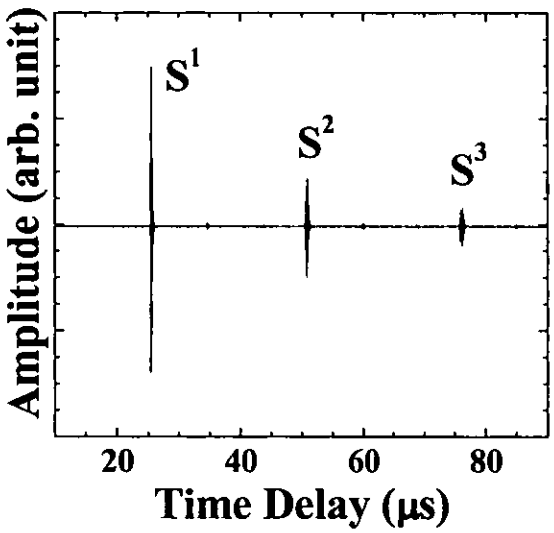

Fig. 4 (a): Makiko Kobayashi, Cheng-Kuei Jen, Yuu Ono, Kuo-Ting Wu and Ishang Shih

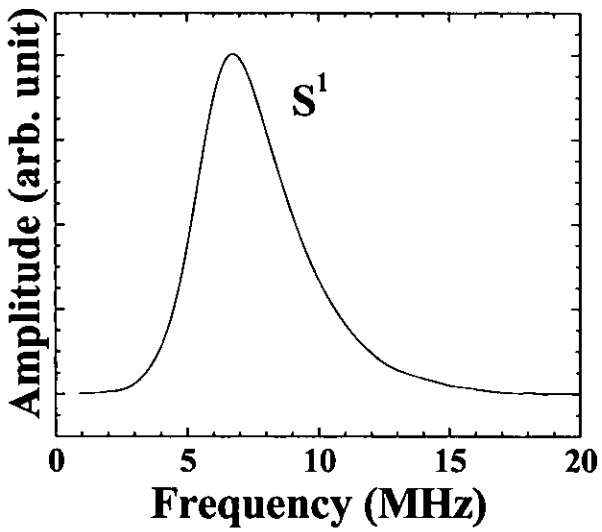

Fig. 4 (b): Makiko Kobayashi, Cheng-Kuei Jen, Yuu Ono, Kuo-Ting Wu and Ishang Shih

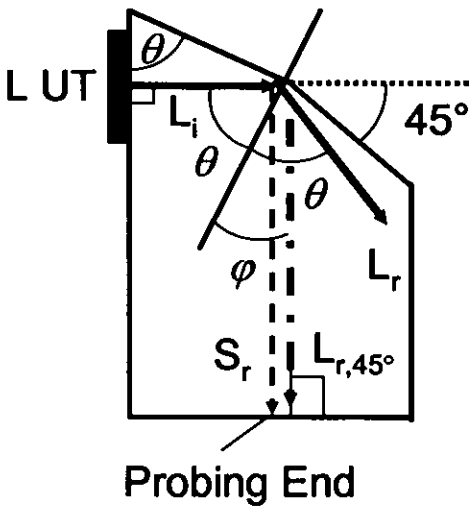

Fig. 5 (a): Makiko Kobayashi, Cheng-Kuei Jen, Yuu Ono, Kuo-Ting Wu and Ishang Shih

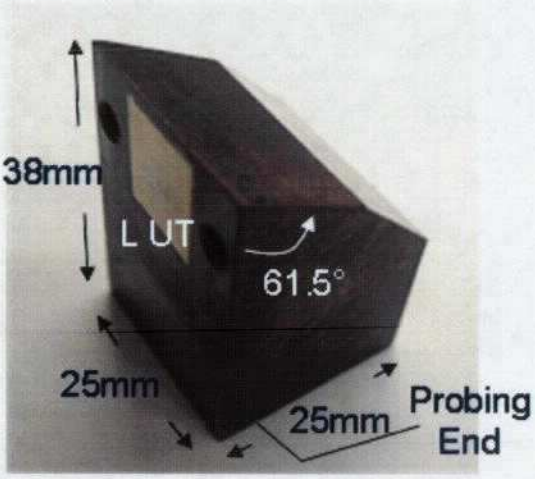

Fig. 5 (b): Makiko Kobayashi, Cheng-Kuei Jen, Yuu Ono, Kuo-Ting Wu and Ishang Shih

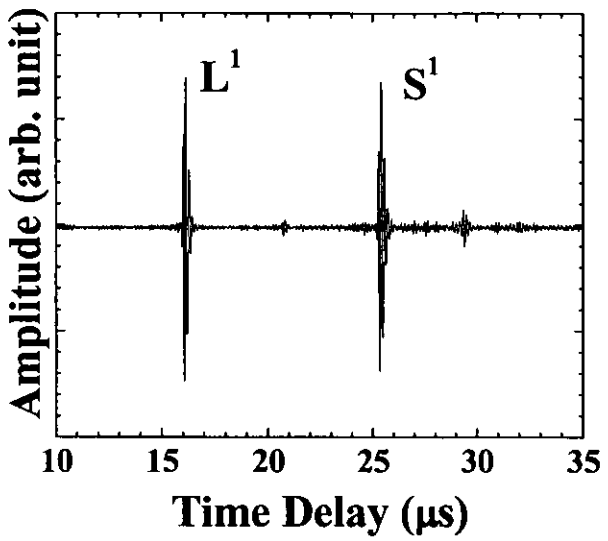

Fig. 6: Makiko Kobayashi, Cheng-Kuei Jen, Yuu Ono, Kuo-Ting Wu and Ishang Shih

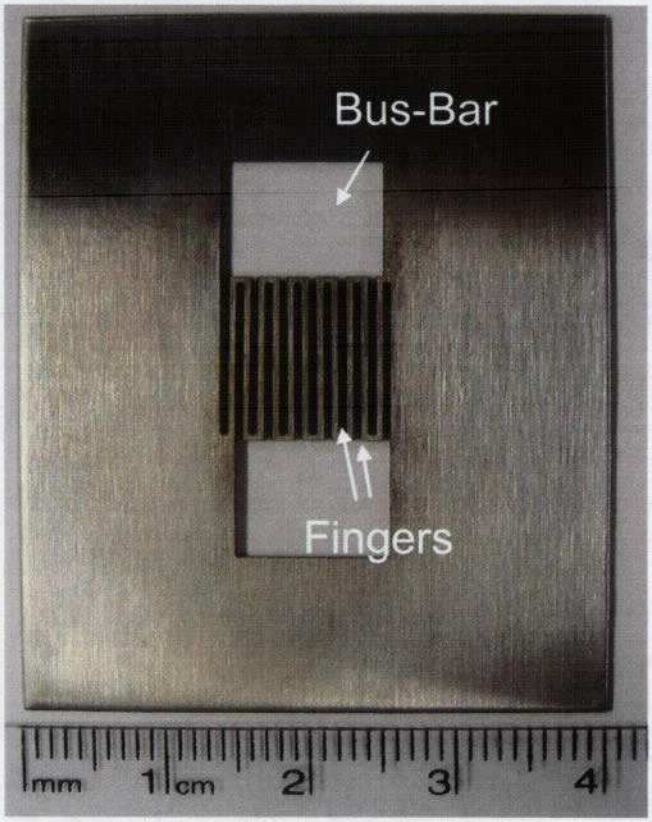

Fig. 7: Makiko Kobayashi, Cheng-Kuei Jen, Yuu Ono, Kuo-Ting Wu and Ishang Shih

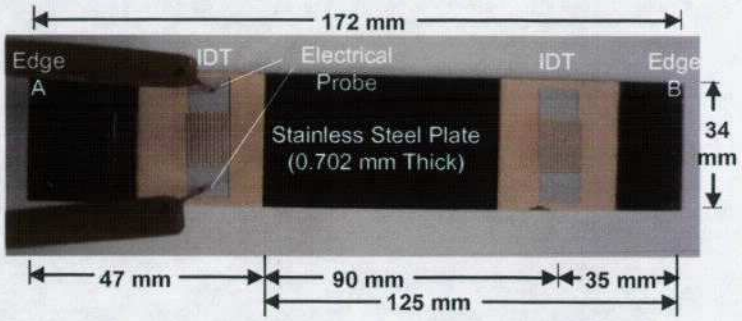

Fig. 8: Makiko Kobayashi, Cheng-Kuei Jen, Yuu Ono, Kuo-Ting Wu and Ishang Shih

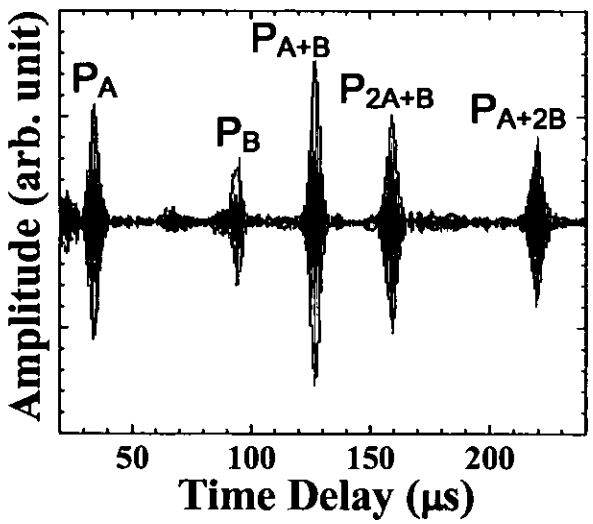

Fig. 9: Makiko Kobayashi, Cheng-Kuei Jen, Yuu Ono, Kuo-Ting Wu and Ishang Shih

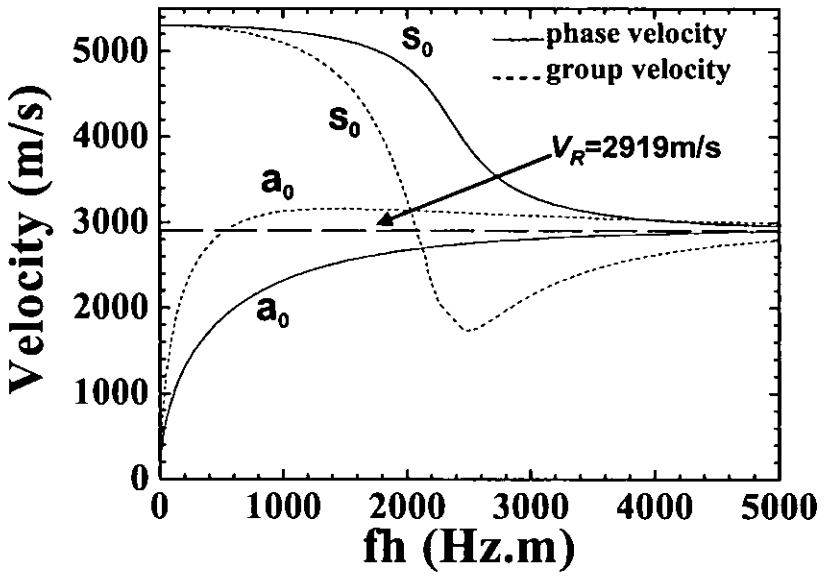

Fig. 10: Makiko Kobayashi, Cheng-Kuei Jen, Yuu Ono, Kuo-Ting Wu and Ishang Shih